

# The AP-1 clathrin adaptor facilitates cilium formation and functions with RAB-8 in *C. elegans* ciliary membrane transport

Oktay I. Kaplan<sup>1</sup>, Anahi Molla-Herman<sup>2,3</sup>, Sebiha Cevik<sup>1</sup>, Rania Ghossoub<sup>2,3</sup>, Katarzyna Kida<sup>1</sup>, Yoshishige Kimura<sup>4</sup>, Paul Jenkins<sup>5</sup>, Jeffrey R. Martens<sup>5</sup>, Mitsutoshi Setou<sup>4</sup>, Alexandre Benmerah<sup>2,3</sup> and Oliver E. Blacque<sup>1,\*</sup>

<sup>1</sup>School of Biomolecular and Biomedical Science, UCD Conway Institute, University College Dublin, Belfield, Dublin 4, Ireland

<sup>2</sup>Institut Cochin, Université Paris Descartes, CNRS UMR 8104, Paris, France

<sup>3</sup>INSERM, U1016, Paris, France

<sup>4</sup>Department of Molecular Anatomy, Hamamatsu University School of Medicine, 1-20-1 Handayama, Hamamatsu, Shizuoka 431-3192, Japan

<sup>5</sup>Department of Pharmacology, University of Michigan, Ann Arbor, MI 48109-5632, USA

\*Author for correspondence ([oliver.blacque@ucd.ie](mailto:oliver.blacque@ucd.ie))

Accepted 6 August 2010

Journal of Cell Science 123, 3966–3977

© 2010. Published by The Company of Biologists Ltd

doi:10.1242/jcs.073908

## Summary

Clathrin adaptor (AP) complexes facilitate membrane trafficking between subcellular compartments. One such compartment is the cilium, whose dysfunction underlies disorders classified as ciliopathies. Although AP-1 $\mu$  subunit (UNC-101) is linked to cilium formation and targeting of transmembrane proteins (ODR-10) to nematode sensory cilia at distal dendrite tips, these functions remain poorly understood. Here, using *Caenorhabditis elegans* sensory neurons and mammalian cell culture models, we find conservation of AP-1 function in facilitating cilium morphology, positioning and orientation, and microtubule stability and acetylation. These defects appear to be independent of IFT, because AP-1-depleted cells possess normal IFT protein localisation and motility. By contrast, disruption of *chc-1* (clathrin) or *rab-8* phenocopies *unc-101* worms, preventing ODR-10 vesicle formation and causing misrouting of ODR-10 to all plasma membrane destinations. Finally, ODR-10 colocalises with RAB-8 in cell soma and they cotranslocate along dendrites, whereas ODR-10 and UNC-101 signals do not overlap. Together, these data implicate conserved roles for metazoan AP-1 in facilitating cilium structure and function, and suggest cooperation with RAB-8 to coordinate distinct early steps in neuronal ciliary membrane sorting and trafficking.

**Key words:** *C. elegans*, RAB-8, Cilia, Clathrin adaptor 1, Membrane transport

## Introduction

Cell polarisation is required for many distinct cellular functions, including differentiation, morphogenesis and proliferation. A neuron, for example, possesses axons and dendrites, which are structurally and functionally distinct. Establishment of specific cellular compartments involves coordinated actions of several events, including trafficking of membrane and cell signalling molecules and asymmetrical arrangement of the cytoskeleton. Recently, primary cilia have emerged as a structurally and functionally distinct sensory and signalling (e.g. sonic hedgehog; Shh) compartment, linked to the molecular pathogenesis of various human conditions including autosomal dominant polycystic kidney disease (ADPKD) and *retinitis pigmentosa*, as well as pleiotropic disorders such as Bardet–Biedl syndrome (Badano et al., 2006; Blacque and Leroux, 2006; Eggenschwiler and Anderson, 2007). Although much has been learned about cilium structure, function and pathogenesis over the past decade, the precise molecular basis of cilium biogenesis, as well as the mechanisms underlying polarised distribution of proteins to cilia, remains poorly understood.

Cilia extend from the surfaces of most eukaryotic cells and consist of a microtubule backbone surrounded by ciliary (plasma) membrane with distinct protein and lipid composition (Vieira et al., 2006). Numerous membrane proteins and signalling molecules are enriched in cilia, indicating the existence of specific ciliary delivery systems. One such system is intraflagellar transport (IFT)

(Blacque et al., 2008), an evolutionarily conserved kinesin-2 and cytoplasmic dynein-dependent bidirectional motility (non-vesicular) of protein complexes along ciliary axonemes, which is thought to build and maintain cilia by delivering ciliary protein cargos. For example, in *Caenorhabditis elegans*, ciliary transmembrane proteins have been observed to undergo IFT (Qin et al., 2004), and IFT regulates the ciliary abundance of PKD-2 (polycystin-2 homologue) (Bae et al., 2006). Outside cilia, membrane-trafficking components are implicated in upstream or earlier-targeting steps. These include AP-1  $\mu$ 1 (clathrin adaptor 1 subunit), Rab8, rabaptin5, PACS-1 and Rab11 (Bae et al., 2006; Deretic et al., 1995; Dwyer et al., 2001; Mazelova et al., 2009a; Moritz et al., 2001; Nachury et al., 2007; Omori et al., 2008). These observations implicate a cooperative relationship between vesicular transport and IFT in targeting proteins to cilia, where membrane trafficking drives upstream transport to the ciliary base, followed by IFT-mediated distribution within cilia. Indeed, evidence for a two-step pathway has already been proposed in numerous systems, including *C. elegans* sensory neurons (Bae et al., 2006).

Clathrin adaptor (AP) complexes have highly conserved roles in vesicular transport, and are essential for life in many organisms. Four distinct heterotetrameric complexes exist (AP-1–AP-4), each consisting of four subunits ( $\alpha, \gamma, \delta, \epsilon$ ;  $\beta 1$ – $\beta 4$ ;  $\mu 1$ – $\mu 4$ ;  $\sigma 1$ ) that possess specific functions within the complex and all individually required for complex stability (Borck et al., 2008; Hinrichsen et al., 2003;

Motley et al., 2003). AP complexes function in vesicle formation by driving recruitment and polymerisation of clathrin coats at target membranes and in cargo sorting by direct or indirect interaction with cytoplasmic-tail sorting signals (Traub, 2009). AP complexes have distinct and varied functions in different cellular compartments. AP-2 ( $\alpha$ - $\beta$ 2- $\mu$ 2- $\sigma$ 2) is required for the assembly of clathrin-coated pits at plasma membranes (Hinrichsen et al., 2003; Motley et al., 2003), whereas AP-1 ( $\gamma$ - $\beta$ 1- $\mu$ 1- $\sigma$ 1) typically functions at the *trans*-Golgi network (TGN) and controls sorting to basolateral plasma membranes (Folsch et al., 1999). A number of findings implicate AP-1 in protein trafficking to cilia. In *C. elegans*, loss of *unc-101* function (AP-1  $\mu$ 1) causes ciliary transmembrane protein mislocalisation and defects in cilium formation (Bae et al., 2006; Dwyer et al., 1998; Ou et al., 2007), and in *Leishmania*, AP-1 mutants fail to assemble flagella (Vince et al., 2008). However, the molecular and conserved basis of AP-1-mediated ciliary functions has not been addressed in detail and components that function with AP-1 to deliver ciliary proteins remain unknown.

Here, we address the cilia-related functions of AP-1 in *C. elegans* (sensory neuronal cilia) and mammalian cell culture and find that they have conserved roles in defining the ciliary compartment. We also show that disruption of AP-1, *rab-8* and the clathrin heavy chain results in identical mis-sorting of a ciliary transmembrane protein (ODR-10) to all plasma membrane destinations. Together with subcellular localisation and protein transport data, our findings suggest that in *C. elegans* sensory neurons, AP-1 and RAB-8 function in a clathrin-dependent manner to mediate distinct early steps in a common ciliary membrane trafficking pathway.

## Results

### *C. elegans* cilium integrity, morphology and positioning requires AP-1 complexes

Cilium integrity was assessed in AP-1 subunit mutants using dye filling. In wild-type (wt) worms, eight pairs of ciliated sensory neurons (six pairs of amphid head cells; PHA/B phasmid tail cells) can incorporate fluorescent dye via environmentally exposed cilia that extend from dendrite tips (Fig. 1A), and dye-filling defects (Dyf) are frequently associated with abnormalities in cilium structure or morphology. Consistent with previous reports (Lee et al., 1994; Ou et al., 2007), *unc-101(sy108)* mutants ( $\mu$ 1 subunit) failed to take up dye (Fig. 1A,B). Transgenic expression of *unc-101::gfp* under an *unc-101* promoter or a ciliated cell-specific promoter (*srb-6p*; expressed in PHA/B/ASH/ADL) rescued the Dyf phenotype, confirming causality by *sy108*, and demonstrating that UNC-101 functions in ciliated cells (Fig. 1A,B). Because mutant alleles for other AP-1 subunit genes are lethal, we used a tissue-specific RNAi protocol (Esposito et al., 2007) and found that knockdown of *aps-1* ( $\sigma$ 1 subunit) in all ciliated cells [using *arl-13p* (Blacque et al., 2005)] or in PHA/B/ASH/ADL only (using *srb-6p*) abolished dye uptake (Fig. 1A,B). As positive control, RNAi knockdown of *unc-101* (PHA/B/ASH/ADL) also abrogated dye uptake (Fig. 1A,B). Because worms have one  $\gamma$ 1,  $\beta$ 1 and  $\sigma$ 1 gene, but two  $\mu$ 1 paralogs (*unc-101*, *apm-1*), we investigated whether *apm-1* influenced cilium integrity. However, this question could not be addressed using mutant alleles (lethal) or RNAi (*apm-1* and *unc-101* sequence similarity is very high); instead, we overexpressed *apm-1::gfp* (with an *unc-101* promoter) in *sy108* worms and found that it rescued Dyf (and Unc) phenotypes (Fig. 1A,B), indicating that *apm-1* overexpression can compensate for *unc-101* loss. However, a transcriptional *apm-1p::gfp* reporter did not appear to be expressed in ciliated cells, but instead was expressed in pharyngeal, intestinal

and hypodermal cells (supplementary material Fig. S1), suggesting that endogenous AP-1 complexes in ciliated cells probably use UNC-101 rather than APM-1.

Next, we directly visualised cilia in AP-1-deficient worms using transcriptional GFP markers, which illuminate individual cilia. Although *unc-101(sy108)* worms form cilia, several defects were found, including truncated axonemes (all cilia), ectopic projections (ASER) and a lack of morphological elaborations such as branches (AWA), forks (AWB) or wings (AWC) (Fig. 1C,D). Similarly, cilia in *aps-1(RNAi)* knockdown worms were truncated and lacked characteristic morphological features (e.g. AWB fork) (Fig. 1C,D). Consistent with these data, analysis of amphid ciliary bundles using GFP-tagged IFT markers, which express in all ciliated cells, also revealed truncated ciliary axonemes in *unc-101* and *aps-1(RNAi)* animals (Fig. 1E); in addition, amphid cilia were frequently misplaced, with some axonemes shifted posteriorly by 5–10  $\mu$ m and others extending sideways or backwards (Fig. 1E, arrows, arrowhead). Because fluorescence images indicated that AP-1 mutant cilia still extended from distal dendrite tips (Fig. 1C,E), posteriorly shifted axonemes probably reflect a dendrite extension phenotype. Finally, we assessed AWB cilium structure in *unc-101* mutant larvae (L2/L3 stage) and found that these cilia were also severely truncated (supplementary material Fig. S2), similarly to adult worms, which suggests that AP-1 drives initial cilium formation, although additional roles in maintenance cannot be ruled out.

Together, these data for two AP-1 subunits, UNC-101 ( $\mu$ 1) and APS-1 ( $\sigma$ 1), indicate that UNC-101-specific AP-1 complexes function in sensory neurons to facilitate cilium formation, morphology and positioning, as well as dendrite extension.

### Ultrastructural analysis of *unc-101* amphid channel cilia

Next, we used transmission electron microscopy (TEM) to investigate amphid channel cilium ultrastructure in *unc-101(sy108)* mutants. In wt worms, ten axonemes extended 7–9  $\mu$ m from distal dendrite tips, possessing  $\sim$ 3  $\mu$ m distal segments (nine singlet microtubules; Fig. 2A,B), then  $\sim$ 4  $\mu$ m middle segments (nine doublet microtubules; Fig. 2F,G,K,L), followed by  $\sim$ 1  $\mu$ m transition zones (constriction of doublet microtubules; Y-link membrane connections; Fig. 2P,Q), and anchored in distal dendrites via transitional fibers (Fig. 2U,V). By contrast, in distal regions of *unc-101* amphid pores, ciliary axonemes were typically absent (Fig. 2C,D). In more proximal pore regions, axonemes were still missing (Fig. 2H,M) and in those that were present, microtubule doublets were frequently missing or misplaced (Fig. 2I,J,N). In addition, amphid pores appeared to be poorly formed, with accumulation of electron-dense material in distal regions (Fig. 2D, arrows); there was also an additional membrane surrounding many ciliary axonemes (Fig. 2I,J,N; arrowhead), which was possibly the membrane of the supporting sheath cell (Fig. 2Z). In deeper sections, most *unc-101* transition zones (TZ) appeared normal (Fig. 2T), although microtubule doublets were sometimes misplaced (Fig. 2Y, arrow). In addition, and consistent with the fluorescence data (Fig. 1E), cilium structure (e.g. TZ) was found in deep sections (+12  $\mu$ m), reflecting the misplaced nature of cilia in *unc-101* worms (Fig. 2R,W,Y). These TZs were not buried within distal dendrites, indicating that cilium misplacement is due to incomplete dendritic extension and not cilium-anchoring defects at dendrite tips. In summary, *unc-101* amphid channel cilia are severely truncated (lacking distal segments), misplaced and possess axonemal microtubule defects.

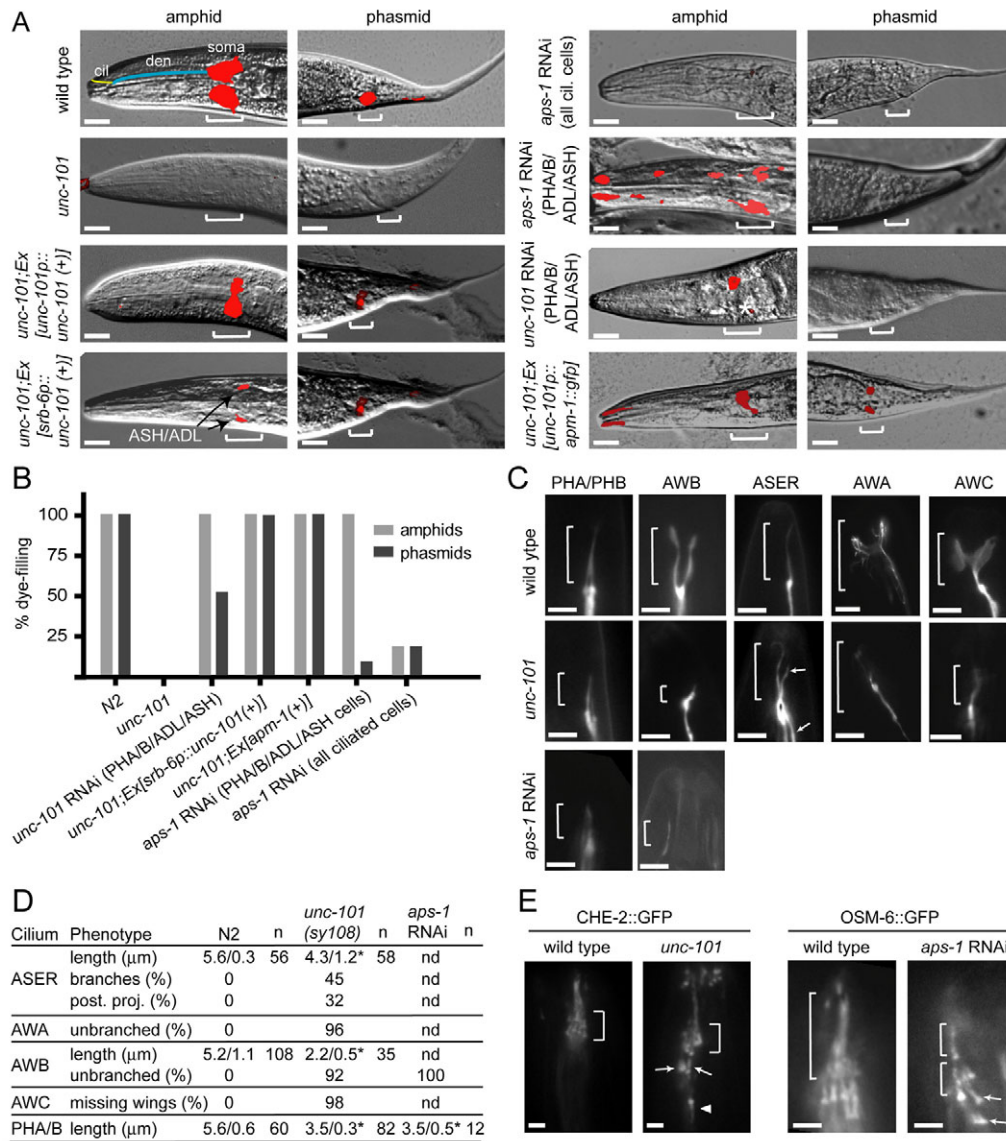


**Fig. 1. *C. elegans* AP-1 complex is required for cilium formation, morphology and positioning.** (A) AP-1 subunit genes (*unc-101*;  $\mu 1A$ , *aps-1*;  $\sigma 1$ ) function in ciliated cells to maintain normal dye-filling. Shown are merged DIC-fluorescence images following a DiI (red fluorescence) incorporation assay. Also denoted in top-left wild-type image is the position of environmentally exposed cilium (cil; yellow) at the distal tips of dendrites (den; blue). *unc-101* (*sy108*) mutants and *aps-1* (RNAi) worms (all ciliated cells); using *arl-13* promoter-driven sense/antisense genomic fragments) possess strong Dyf defects in amphids and phasmid neurons (brackets). Also, *unc-101* (RNAi) and *aps-1* (RNAi) animals [using sense and antisense genomic fragments expressed under the *srb-6* promoter, active only in PHA/B/ADL/ASH ciliated cells. (Troemel et al., 1995)] show severely reduced dye uptake in PHA/B and in some amphid cells (presumably ADL/ASH; asterisk). Dye-filling is restored in *unc-101* (*sy108*) mutants expressing *unc-101::gfp* (under endogenous *unc-101* promoter or ciliated cell-specific *srb-6* promoter) or *apm-1::gfp* (under an *unc-101* promoter). As expected, rescue using *srb-6*-driven construct is restricted to PHA/B/ADL/ASH ciliated cells. Scale bars: 10  $\mu$ m. (B) Analysis of dye-filling data from A. Percentage of worms with a dye-uptake defect. Note that for *unc-101* and *apm-1* RNAi strains (knockdown in PHA/B/ADL/ASH), amphid dye-filling was only grossly scored; detailed analysis would probably also uncover Dyf defects in ADL/ASH.  $n > 50$  worms. (C) *unc-101* worms possess defective cilium morphologies. Shown are fluorescence images of *unc-101* (*sy108*) worms expressing ciliated cell-specific transcriptional GFP markers; *srb-6p::gfp* (PHA/B), *str-1p::gfp* (AWB), *gcy-5p::gfp* (ASER), *gpa-6p::gfp* (AWA) and *str-2p::gfp* (AWC). Scale bars: 3  $\mu$ m. (D) Cilium morphology analysis from N2, *unc-101* (*sy108*) and *aps-1* (RNAi) (all ciliated cells) animals. Cilium lengths shown as mean with s.d. \* $P < 0.001$ ; nd, not determined; n, number of cilia assessed. (E) Cilia are mispositioned in *unc-101* worms. Fluorescence images of one amphid cilium bundle in N2, *unc-101* (*sy108*) and *aps-1* (RNAi) (all ciliated cells) worms expressing IFT transgenes. Arrows, mispositioned cilia; arrowhead, cilium extending backwards; bracket, amphid ciliary bundle. Scale bars: 2  $\mu$ m.

### Assessment of microtubule post-translational modification in *unc-101* worms

We hypothesised that the ultrastructural microtubule defects of *unc-101* worms might reflect microtubule destabilisation caused by post-translational modification (PTM) abnormalities. Using

immunostaining, reduced polyglutamylation signals were found in *unc-101* amphid channel cilia (supplementary material Fig. S3A); however, we also observed reduced alpha-tubulin ( $\alpha$ Tub) signals in *unc-101* cilia (supplementary material Fig. S3A), indicating that a specific polyglutamylation defect is unlikely in these worms;

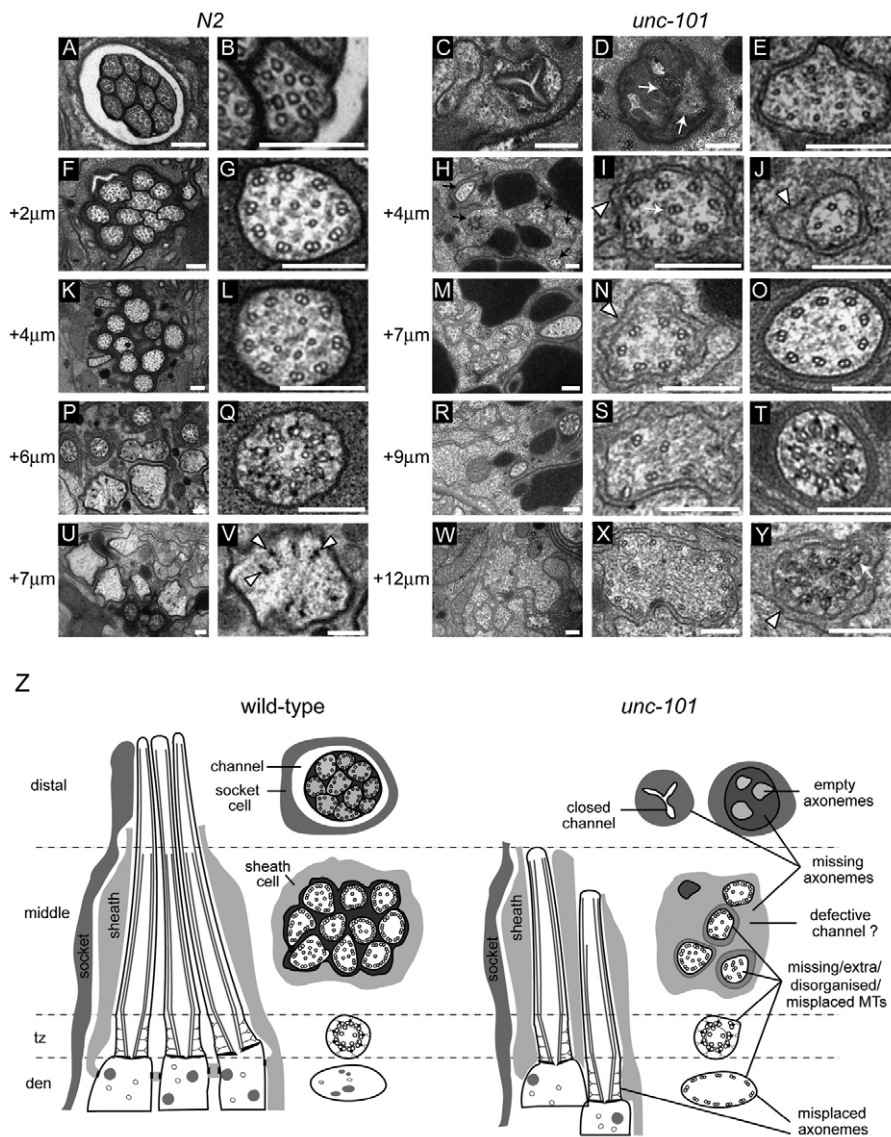


**Fig. 2. TEM analysis of *unc-101* mutants reveals abnormalities in amphid pore formation, axonemes and ciliary microtubules.** Shown are low and high magnification images from TEM serial cross sections of amphid channel cilia from *N2* and *unc-101*(*sy108*) animals. (A–E) Distal region of amphid pore. *N2* worms possess ten-singlet microtubule (MT)-containing axonemes (A,B), whereas axonemes are missing or degenerate and lacking MT structure in *unc-101* mutants (C,D). Occasionally, an axoneme adjacent to the amphid pore is observed in *unc-101* animals (E). Also, the amphid pore appears poorly formed and filled with electron dense material (arrows). (F–L) Sections 2–4 μm proximal to A–E through middle segment (MS) region of pore. Instead of ~12 axonemes containing nine outer-doublet MTs (F,G,K,L), many axonemes are missing in *unc-101* mutants (H). Axonemes that are present often exhibit missing or disorganised doublet MTs (I,J) and are surrounded by an additional membrane (I,J,N; arrowheads), which might belong to the supporting sheath cell and indicate abnormal structural arrangements between neuronal cilia and the sheath cell (see Z). (M–Q) Sections 6–7 μm proximal to A–E through MS, transition zone (TZ) and transition fiber (TF) regions. Although most *N2* ciliary axonemes exhibit TZ and TF structure at this point (P,Q), many ciliary axonemes in *unc-101* worms still display middle segment type structure (N,O), indicating posteriorly shifted axonemes. Some *unc-101* axonemes possess nine doublet MTs (O); however, in others, MTs are missing (M). (R–Y) Sections 7–12 μm proximal to A–E through TF region (U,V). Unlike *N2* worms, where cilia are not observed beyond +8 to +9 μm, axonemal ultrastructure (e.g. MS, TZ) is found beyond this point in *unc-101* animals (W–Y). Although *unc-101* TZs are typically normal (T), misplaced MT doublets and an additional enveloping membrane (Y, arrowhead) are also sometimes observed (Y, arrow). (Z) Schematics of amphid channel cilia (longitudinal and transverse views) from *N2* and *unc-101* worms showing the major ultrastructural defects observed (not to scale; e.g. some *unc-101* cilia shifted more posteriorly than indicated). Scale bars: 200 nm.

instead, and consistent with our TEM data, the reduced signals might reflect a partial loss of ciliary axonemal tubulin; alternatively, the dispersed nature of amphid cilia in *unc-101* worms (Fig. 1E) might indirectly cause the appearance of reduced tubulin staining. Although ciliary acetylated  $\alpha$ -tubulin (AcTub) could not be assessed (wt cilia are not acetylated; supplementary material Fig. S3B), non-ciliary AcTub levels and AcTub: $\alpha$ Tub ratios were elevated in the anterior processes of *unc-101* non-ciliated ALM touch-sensing (mechanosensory) neurons (supplementary material Fig. S3B,C). These data indicate that although ciliary microtubule PTM may not be affected, *unc-101* worms might possess AcTub defects in non-ciliary regions of sensory neurons.

### Mammalian AP-1 complex influences cilium shape, orientation and microtubule acetylation

Using siRNA against  $\gamma$ -adaplin to disrupt AP-1 complexes (Borck et al., 2008), we assessed whether mammalian AP-1 is required for primary cilium integrity in htert-RPE1 cells. Efficient depletion of AP-1 was confirmed by western blot (supplementary material Fig. S4A) and immunofluorescence (supplementary material Fig. S4B).

Although ciliogenesis per se was not affected in AP-1-depleted cells, with the number of ciliated cells similar to control cells (Fig. 3A), defects in cilium positioning and orientation were observed. In basic cell culture conditions, RPE1 cilia grew parallel to adherent surfaces, with a confined Z-axis distribution, resulting in cilia appearing within the same focal plane (Molla-Herman et al., 2010). However, in AP-1-depleted cells, cilia were observed over three to four focal planes, indicating a more random distribution. To study this further, 3D reconstructed images were generated and cilium length, positioning and morphology analysed. Although cilia from control cells were homogeneously rod-like, cilia in AP-1-depleted cells harboured different phenotypes. First, 50% of cilia possessed curved shapes (twisted) and discontinuous acetylated  $\alpha$ -tubulin staining (Fig. 3B,C), which was not due to breaks in ciliary microtubules, because immunostaining against polyglutamylated microtubules revealed a continuous axonemal staining pattern (supplementary material Fig. S5). Second, average cilium length was longer ( $3.5 \pm 1.8 \mu\text{m}$ ;  $P < 0.01$ ) than that in control cells ( $2.8 \pm 0.7 \mu\text{m}$ ) (Fig. 3D). Third, although cilia from control cells were almost parallel to the adhesion substrate ( $-2.6 \pm 7.5^\circ$ ), the average angle

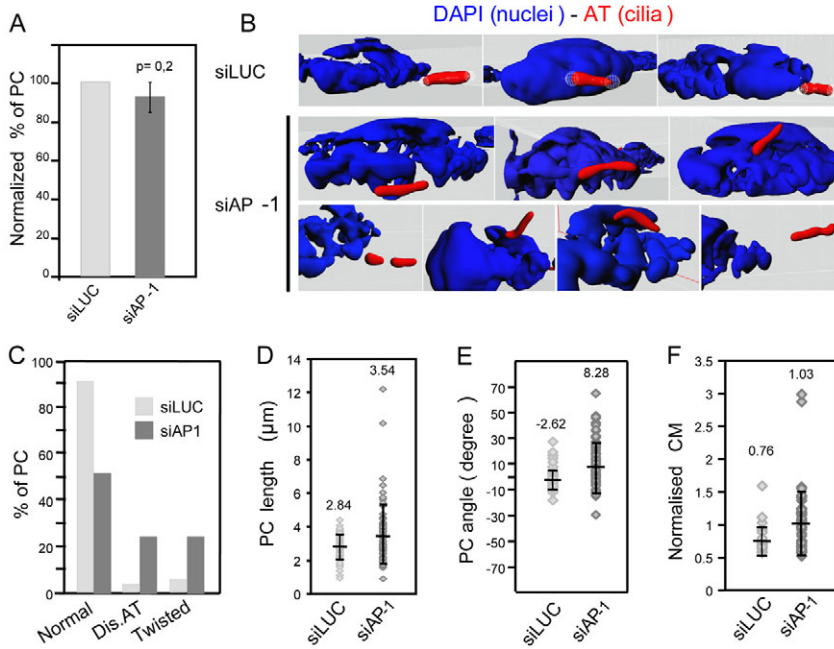


**Fig. 3. AP-1-depleted mammalian cells possess primary cilium defects.** RPE1 cells transfected with control siRNA (luciferase; siLUC) or siRNA targeting  $\gamma$ -adaptn (siAP-1). (A) AP-1-depleted cells form cilia. Percentage of ciliated cells normalised to siLUC-treated cells. Mean  $\pm$  s.d.;  $n=700$  cells, three independent experiments. (B–F) Loss of AP-1 function disrupts cilium morphology, position or orientation, and microtubule acetylation. Shown in B are 3D reconstructions stained with acetylated tubulin (AT) (cilium, red) and DAPI (nucleus, blue) from deconvoluted Z-stack images. Quantification of cilium phenotypes (cilia with discontinuous AT staining (Dis. AT), and curved or twisted cilia) are shown in C and cilium length ( $\mu\text{m}$ ) is shown in D. Spread of angles formed by cilia with adhesion surface is shown in E. Shown in F is the centre of mass (CM) of each cilium normalised to that of its corresponding nucleus. For each assay,  $n=70$ ; three independent experiments. Means  $\pm$  s.d. are shown.

formed by cilia with the adherent surface in AP-1-depleted cells was more variable ( $8.3 \pm 19.6^\circ$ ;  $P < 0.0001$ ), indicating more random cilium orientation (Fig. 3E). Finally, by analysing the cilium position relative to the nucleus, cilium distribution in space was found to be affected in AP-1-depleted cells. In control cells, the cilium lay slightly below the centre of mass of the nucleus (normalised centre of mass =  $0.8 \pm 0.2$ ), indicating an alignment with the lower part of the nucleus (Fig. 3F). By contrast, in AP-1-depleted cells, the nuclear alignment of the cilium was more random (normalised centre of mass =  $1.0 \pm 0.5$ ;  $P < 0.001$ ), with greater variation (Fig. 3F). In summary, AP-1-depleted mammalian cells possess defects in cilium morphology (longer, curved), positioning or orientation and ciliary microtubule acetylation. Although phenotypically not identical, these findings are consistent with our worm data, hence we conclude that AP-1 has a conserved role in defining the metazoan cilium compartment.

#### Intraflagellar transport is normal in AP-1-depleted cells

The ciliary disruption of AP-1-depleted cells might be explained by defects in intraflagellar transport (IFT). To explore this hypothesis in *C. elegans*, we examined the subcellular localisation and motility of six IFT::GFP proteins in *unc-101* mutants. Specifically, we looked at one IFT-A protein (CHE-11/IFT140), three IFT-B proteins (CHE-2/IFT80, DYF-1/IFT70, IFT-20), and two kinesin-2 motor subunits (KAP-1/kinesin II, OSM-3/KIF17), chosen because of their differential contributions to IFT in *C. elegans* (Blacque et al., 2008). In all cases, IFT protein localisation was grossly normal at the ciliary base and along ciliary axonemes of *unc-101* and *aps-1*(RNAi) worms (Fig. 4A; supplementary material Fig. S6A). Using time-lapse videomicroscopy and kymography, we found that similarly to wt cilia, IFT proteins moved robustly along *unc-101* cilia (Fig. 4A; supplementary material Fig. S6A). Furthermore, in *unc-101* amphid channel cilia middle segments, anterograde IFT rates ( $\sim 0.7 \mu\text{m}/\text{second}$ ) and rate profiles were similar to that in wt animals (supplementary material Table S1, Fig. S6B). Also, in *unc-101* worms, where rare putative distal segments were detectable, anterograde IFT also operated at

wt speeds of  $1.1\text{--}1.2 \mu\text{m}/\text{second}$ . We also watched IFT proteins moving along *unc-101* dendrites and found that unlike ciliary transmembrane proteins ODR-10 and PKD-2, whose dendritic translocations are abolished in *unc-101* mutants (Bae et al., 2006; Dwyer et al., 2001), IFT::GFP proteins moved along *unc-101* dendrites (Fig. 4B; supplementary material Fig. S6C). We also found no difference in anterograde (towards cilium) dendritic translocation rates for CHE-11::GFP in wt ( $0.74 \pm 0.30 \mu\text{m}/\text{second}$ ;  $n=30$ ) and *unc-101* ( $0.74 \pm 0.07 \mu\text{m}/\text{second}$ ;  $n=10$ ) worms. In agreement with the worm data, ciliary localisations of mammalian IFT46 (Fig. 4C), IFT88 (supplementary material Fig. S7) and BBS1 (supplementary material Fig. S5) are normal in AP-1-depleted RPE1 cells.

In addition to confirming that IFT is not affected in AP-1-disrupted cells, the above findings also suggest that AP-1 and IFT function independently in facilitating cilium structure and morphology. To test this notion further, we analysed ASER and PHA/B cilium lengths in double mutants of *unc-101* and IFT genes (*osm-3*, *klp-11* and *osm-5*/IFT88) and found evidence of additive phenotypes. For example, *unc-101*;*osm-3* and *unc-101*;*klp-11* worms possessed a subset of very short cilia ( $< 2 \mu\text{m}$ ), that was not observed in single mutants, and average lengths were reduced (supplementary material Fig. S8A–C,E–G). In addition, double mutant length profiles frequently appeared as a combination of single mutant profiles, displaying the shorter length characteristics of *osm-3* and *osm-5* mutants, yet retaining a broad range of length phenotypes characteristic of *unc-101* mutants (supplementary material Fig. S8A,C,D). These genetic data indicate that *unc-101* mutations are additive to *osm-3*, *klp-11* and *osm-5* mutations, and support the notion that AP-1 functions in a separate pathway to IFT in defining the cilium compartment.

#### Disruption of *chc-1* and *rab-8* phenocopies the cilium integrity and ciliary membrane sorting and transport defects of AP-1-deficient worms

To find genes that function with AP-1 in facilitating cilium formation and ciliary membrane transport, candidate *C. elegans*

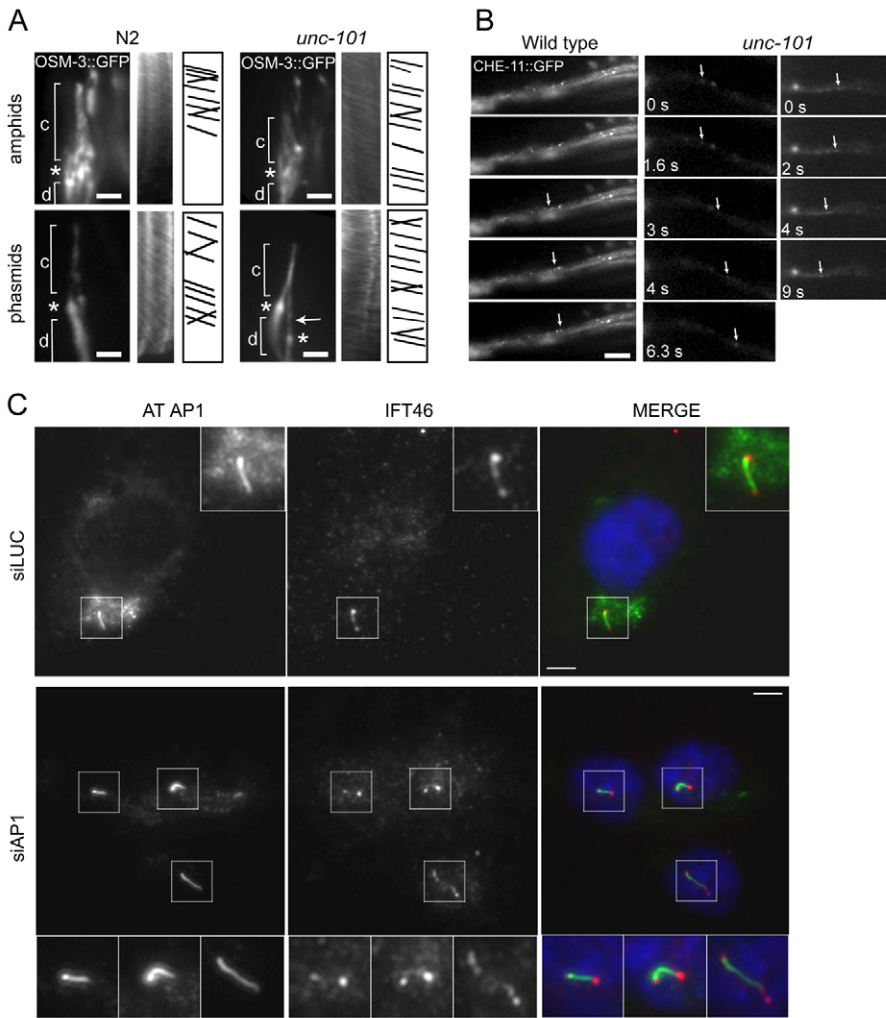


**Fig. 4. Intraflagellar transport is not affected in AP-1-depleted cells.** (A) Fluorescence images of amphid or phasmid cilia in N2 and *unc-101*(*sy108*) worms overexpressing an *osm-3::gfp* transgene. OSM-3 localises normally to ciliary axonemes (c) and at the base of cilia (asterisk) in *unc-101* worms. Note anteriorly shifted phasmid cilium in *unc-101* animals (bottom right; arrow). Kymographs and kymograph schematics, derived from time-lapse movies (3 frames/second), show OSM-3::GFP particles moving anterogradely along *unc-101* cilia. Scale bars: 2  $\mu$ m. (B) Time-lapse fluorescence images of *C. elegans* amphid dendrites showing that similarly to N2 worms, CHE-11::GFP-associated particles (arrow) translocate bidirectionally along *unc-101* dendrites. (C) AP-1-depleted mammalian cells possess normal IFT protein ciliary localisations. RPE1 cells treated with siRNA to knock down  $\gamma$ -adaptin (siAP-1) or luciferase (siLUC; control) and stained for acetylated tubulin (AT, cilia, green), AP-1 ( $\gamma$ -adaptin, green), IFT46 (red) and nuclei (DAPI). Magnifications correspond to ciliary regions. Scale bars: 5  $\mu$ m.

gene mutants were screened for animals that phenocopy *unc-101* worms. Specifically, we looked for mutants that were Dyf and possessed ODR-10-trafficking defects to AWB cilia (Dwyer et al., 2001; Lee et al., 1994; Ou et al., 2007). Candidates were selected from published biochemical and genetic associations with AP-1 complexes (supplementary material Table S2). Using dye-filling as a primary screen, Dyf defects were found for *chc-1*(*b1025ts*) mutants (clathrin heavy chain) and wt animals overexpressing a *rab-8*(*wt*)::*gfp* transgene (expressed via *arl-13* promoter in all ciliated cells) (Fig. 5A; supplementary material Fig. S9). Next, we directly examined cilium structures using GFP markers and found that AWB and PHA/B cilia in *chc-1*(*b1025ts*) mutants were slightly longer ( $P < 0.001$ ) and shorter ( $P < 0.001$ ) compared with cilia in wt worms (Fig. 5B; supplementary material Fig. S10). Also, WT worms overexpressing *gfp::rab-8*(*wt*) possessed moderately truncated PHA/B cilia (supplementary material Fig. S10;  $P < 0.001$ ). Furthermore, and confirming previous findings, WT worms overexpressing *rab-8*(*Q67L*) (GTP-locked dominant active *rab-8* expressed in AWB cells using *str-1* promoter) also possessed short AWB cilia (Fig. 5B;  $P < 0.001$ ) (Mukhopadhyay et al., 2008). Together, although phenotypes were not identical (short cilia in *unc-101*, *gfp::rab-8*(*OverEx*) and *rab-8*(*Q67L*)(*OverEx*) worms versus long or short cilia in *chc-1* mutants), these findings are consistent with a role for *chc-1* and *rab-8* in maintaining cilium

morphology. All other examined mutants were wild type for dye filling, including mutants for genes with strong functional associations with AP-1 (e.g. *arf-1*). Notably, *cltc-1*(*tm3288*) (clathrin light chain) and *rab-8*(*tm2526*) loss-of-function mutants were also wild type for dye filling and possessed normal AWB cilium structure (Fig. 5A,B; supplementary material Fig. S9).

Next, using an *str-1p::odr-10::gfp* transgene (Dwyer et al., 2001), which expresses the transmembrane ciliary odorant receptor ODR-10 in AWB cells, we investigated ODR-10 trafficking in worms with disrupted *chc-1* or *rab-8* functions. As previously reported (Dwyer et al., 2001), in wt worms, ODR-10 accumulated as punctate spots in the AWB cell soma, translocated as discrete particles along the AWB dendrite compartment, and was highly enriched in the AWB ciliary membrane (Fig. 5C). However, similarly to *unc-101* (Dwyer et al., 2001) and *aps-1* (RNAi) worms, ODR-10 was targeted to all plasma membrane destinations and dendritic vesicular transport was abolished in *chc-1* mutants and *rab-8*(*Q67L*)(*OverEx*) animals, as well as in *unc-101;rab-8*(*Q67L*)(*OverEx*) and *unc-101;rab-8*(*tm2526*) worms (Fig. 5C; supplementary material Fig. S11A,B). Consistent with normal cilium integrity in *rab-8* and *cltc-1* mutants, ODR-10 trafficking was normal in these worms (Fig. 5C; supplementary material Fig. S12A).

Finally, loss of ODR-10-associated vesicles, coupled with abnormal routing of ODR-10 to plasma membranes, suggests that

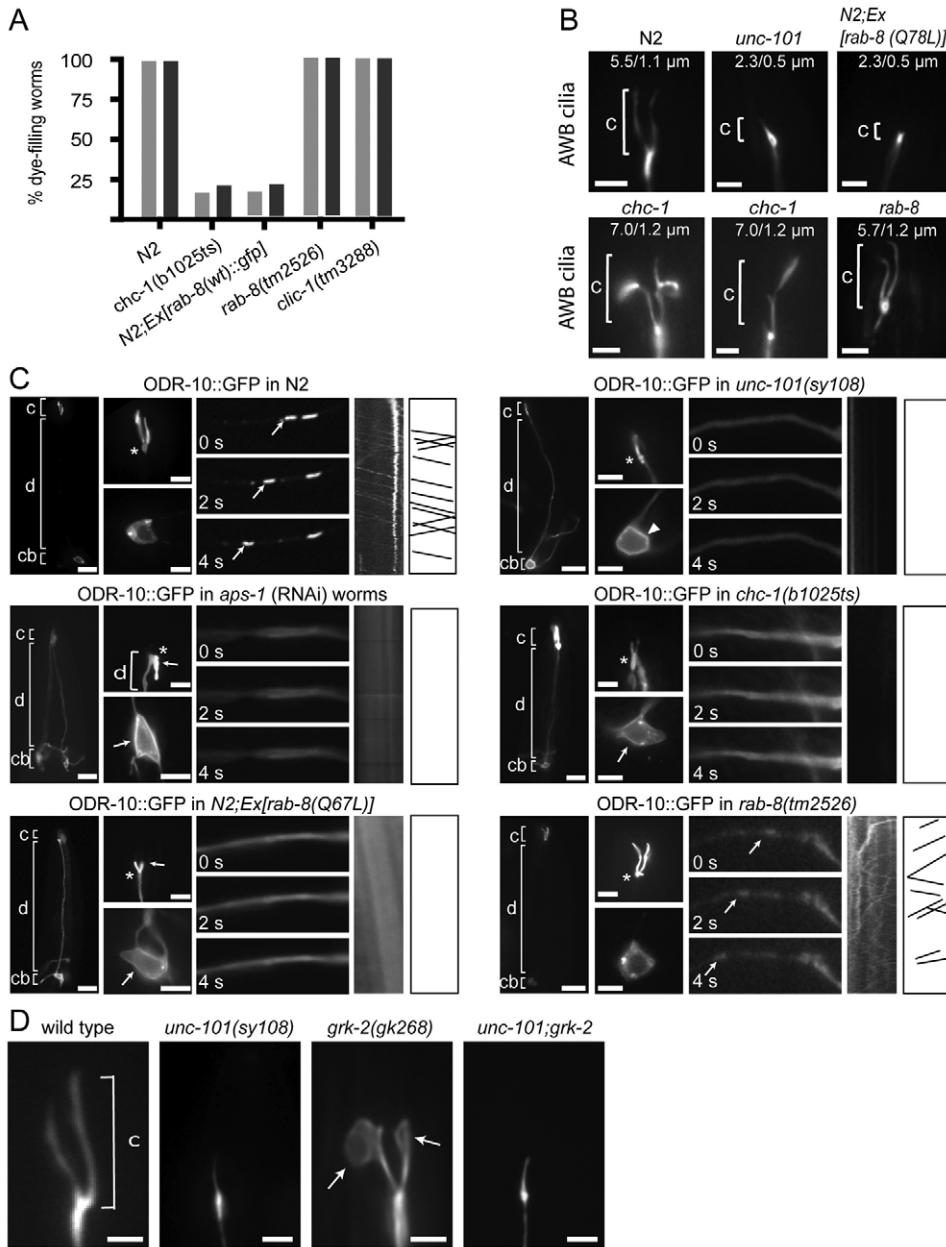


**Fig. 5. Disruption of *C. elegans rab-8* and *chc-1* function phenocopies the cilium formation and ciliary membrane protein transport defects of *unc-101* mutants.**

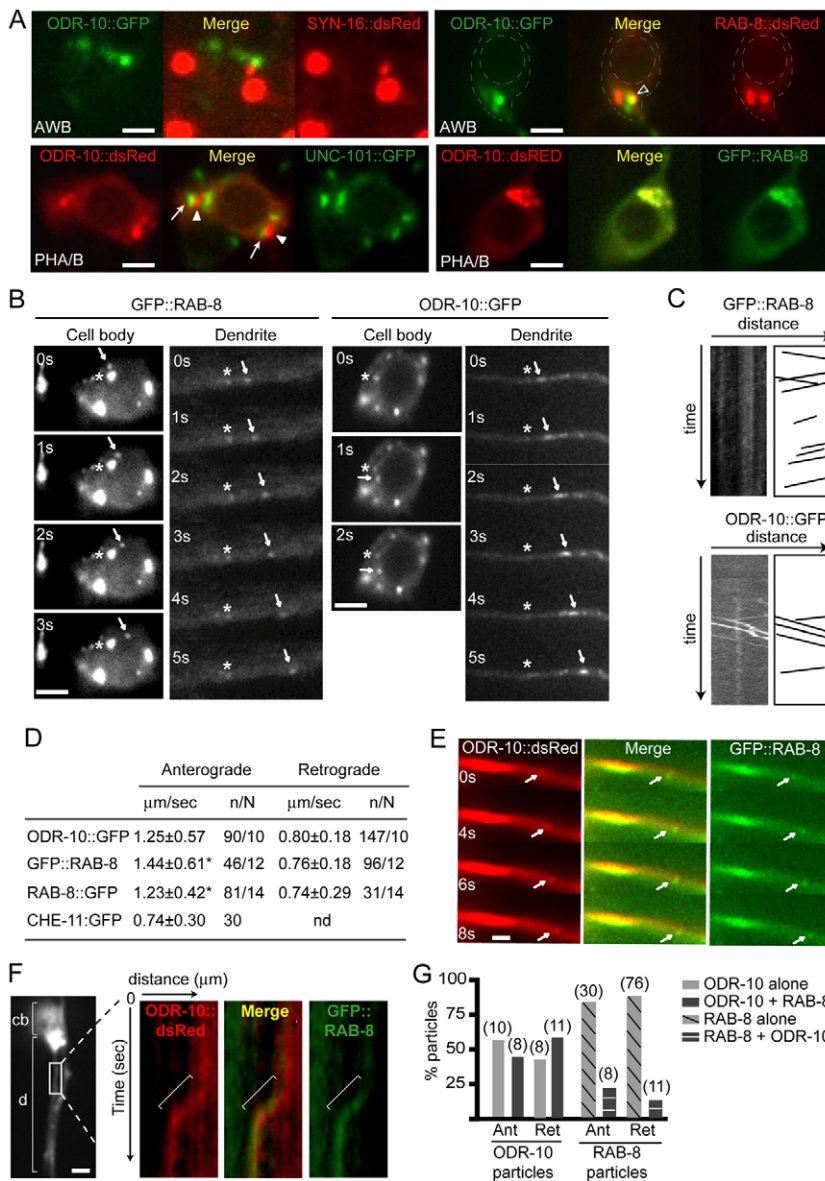
(A) *chc-1* mutants and N2 animals expressing an *arl-13p::rab-8(wt)::gfp* transgene possess dye-filling defects; *rab-8* and *chc-1* loss of function (LOF) mutants are dye-filling normal. Shown is the percentage of animals incorporating Dil in amphid and phasmid neurons. (B) AWB cilium (brackets) morphologies are disrupted in *chc-1(b1025ts)* mutants and N2 worms expressing an *srb-6p::rab-8(Q67L)* transgene [encodes GTP-locked RAB-8 expressed in AWB cells (Mukhopadhyay et al., 2008)], but not in *rab-8(tm2526)* LOF mutants. Images are from worms of indicated genotype expressing the AWB cilium marker, *str-1p::gfp*. Cilium length is indicated as mean/s.d.  $n > 50$ . Scale bars: 3 μm. (C) ODR-10::GFP is abnormally sorted to all plasma membrane destinations and ODR-10 dendritic vesicles fail to form in AP-1 subunit and *chc-1* mutants, and *srb-6p::rab-8(Q67L)*-expressing worms. Fluorescence images of AWB neurons from worms expressing an *odr-10::gfp* transgene. Presented for each strain is a low magnification AWB image [left, showing entire cell with cilium (c), dendrite (d) and cell body (cb) denoted] and two smaller high-magnification images, showing AWB cilium (top image; asterisk denotes cilium base) and cell body (bottom image). Also shown are three images of AWB dendrite (third from left) from a time-lapse movie (s, seconds), as well as corresponding kymographs (second from right) and kymograph schematics (right). Arrowhead denotes ODR-10 at plasma membrane. Scale bars: 10 μm (left panels) and 3 μm (all other panels). (D) Expansion of AWB ciliary membrane in *grk-2(268)* mutants requires *unc-101*. Fluorescence images of worms expressing an *str-1p::gfp* transgene. Arrows denote large membrane fans at tips of AWB cilium forks. Scale bars: 2 μm.

membrane flow to cilia is defective in *rab-8* and *unc-101* disrupted worms. Indeed, *C. elegans rab-8* is required for the formation of abnormally large membranous fans at the distal tips of AWB cilia in odorant signalling mutants (e.g. *grk-2(gk268)* worms) (Mukhopadhyay et al., 2008). To assess whether *unc-101* functions in a similar fashion, we investigated AWB fan morphology in *unc-101;grk-2* worms and found suppression of AWB cilium fan formation (Fig. 5D).

Together, these data implicate overlapping roles for *unc-101*, *chc-1* and *rab-8* in maintaining cilium integrity, ciliary transmembrane protein sorting and trafficking, and membrane addition to *grk-2* mutant AWB cilia. Furthermore, the identical misrouting of ODR-10 to all plasma membrane destinations in *unc-101/aps-1(RNAi)*, *rab-8(Q67L)(OverEx)* and *unc-101;rab-8(Q67L)(OverEx)* animals suggests that AP-1 complexes and RAB-8 function at early steps of a common ciliary membrane transport pathway.

#### AP-1 and RAB-8 function at distinct steps in trafficking ciliary membrane proteins

To further explore AP-1 and RAB-8 function in an ODR-10 ciliary membrane trafficking pathway, we examined their subcellular localisations in *C. elegans* sensory neurons using fluorescent-protein-tagged transgenes driven in AWB (*str-1* promoter) or PHA/B (*srb-6* or *arl-13* promoters) ciliated cells. For ODR-10::GFP (AWB), ODR-10::dsRed (PHA/B), UNC-101::GFP (PHA/B), GFP::RAB-8 (PHA/B) and RAB-8::dsRed (AWB), punctate perinuclear signals were observed (Fig. 6A), which is consistent with early sorting of ODR-10 by AP-1 or RAB-8 in the cell soma. In addition, ODR-10 and RAB-8 (N- and C-terminal tagged) localised to AWB and PHA/B cilia (supplementary material Fig. S13A,B); however, no specific UNC-101::GFP signals were found at ciliary structures, and in dendrites, signals were mostly diffuse, with only a few visible (and faint) punctuate spots, suggesting that



UNC-101 functions mostly in the cell soma (supplementary material Fig. S13C). To investigate further the cell soma localisations, we made double transgenic animals expressing red and green-tagged transgenes. First, we found that ODR-10 (AWB) did not colocalise with the TGN-localised SNARE protein SYN-16 (Chun et al., 2008) (Fig. 6A). Next, we observed that ODR-10 and UNC-101 cell soma signals (PHA/B cells) were juxtaposed and did not overlap, whereas many, if not most, ODR-10 and RAB-8 signals colocalised (Fig. 6A; supplementary material Movies 1, 2).

Using time-lapse videomicroscopy, GFP::RAB-8 (and RAB-8::dsRed) signals were found to translocate in cell somas and along dendrites (Fig. 6B), with the latter reminiscent of ODR-10 dendritic trafficking (Dwyer et al., 2001). Similarly to ODR-10::GFP, GFP::RAB-8 signals also moved over long dendrite distances and in both directions (Fig. 6C; kymographs). By contrast, UNC-101-associated particles that moved were very rarely detected. Kymographic analyses of dendritic time-lapse movies determined

**Fig. 6. Subcellular localisation and motility behaviours of AP-1 subunit, RAB-8 and ODR-10 in *C. elegans* sensory neurons.** (A) ODR-10 colocalises with RAB-8 in cell soma, whereas ODR-10 and UNC-101/TGN signals are juxtaposed and do not overlap. Shown are green, red and merged fluorescence images of AWB or PHA/B cell soma from worms expressing the indicated transgenes. SYN-16::dsRed marks TGN. Arrows, UNC-101::GFP; arrowheads (closed), ODR-10::dsRed; arrowhead (open), colocalised ODR-10::GFP and RAB-8::dsRed. Scale bars: 2  $\mu\text{m}$ . (B, C) RAB-8 and ODR-10 translocate in cell soma and dendrites.

Individual frames from fluorescence time-lapse recordings in worms expressing *srb-6p::gfp::rab-8* (PHA/B cells) or *str-1p::odr-10::gfp* (AWB cells). s, seconds. Arrows, moving particles; asterisk, non-moving reference point. C shows kymographs and kymograph schematics from dendritic time-lapse movies in B, with particles moving in both directions. Scale bars: 2  $\mu\text{m}$ .

(D) Anterograde (towards cilium) and retrograde (towards cell soma) velocities of ODR-10::GFP (AWB), GFP::RAB-8 (PHA/B) and RAB-8::GFP (AWB) moving along dendrites. Velocities derived from multiple kymographs (N), n, number of particles measured. \*, pairwise comparisons (using *t*-test analysis) of anterograde ODR-10 rates with anterograde GFP::RAB-8 ( $P=0.041$ ) and RAB-8::GFP ( $P=0.384$ ) rates. (E–G) Moving dendritic vesicles containing ODR-10 also contain RAB-8. Shown in E and F are red, green and merged images from time-lapse movies (time shown in seconds) of PHA/B dendrites in worms expressing *srb-6p::odr-10::dsRed* and *arl-13p::gfp::rab-8* transgenes. Green and red images simultaneously acquired using an image beam splitter. Arrow, anterograde (towards cilium)-moving particle containing ODR-10 and RAB-8. Shown in F is a kymograph derived from a dendritic time-lapse movie, focusing on a specific section of one of the PHA/B dendrites. Note perfect overlap of a retrograde (towards cell body) moving ODR-10 and RAB-8 marked vesicle (bracket). cb, cell soma; d, dendrites. G is a merged kymograph analysis showing % ODR-10::dsRed lines colocalising with GFP::RAB-8 lines (ODR-10 + RAB-8) or not (ODR-10 alone). Also shown is % GFP::RAB-8 lines colocalising with ODR-10::dsRed lines (RAB-8 + ODR-10) or not (RAB-8 alone). Data for anterograde (Ant) and retrograde (Ret) moving particles is shown. Number of lines counted for each category is shown in parentheses. Scale bars: 3  $\mu\text{m}$  (E), 5  $\mu\text{m}$  (F).

that RAB-8::GFP (PHA/B cells) and GFP::RAB-8 (PHA/B cells) moved anterogradely (towards the cilium) at average speeds of  $\sim 1.23$  and  $\sim 1.44$   $\mu\text{m}/\text{second}$ , respectively, and retrogradely (towards the cell body) at average speeds of  $\sim 0.74$  and  $\sim 0.76$   $\mu\text{m}/\text{second}$ , respectively (Fig. 6D). Interestingly, these speeds are comparable with ODR-10::GFP (AWB cells), which moves at  $\sim 1.25$   $\mu\text{m}/\text{second}$  (anterograde) and  $\sim 0.80$   $\mu\text{m}/\text{second}$  (retrograde) (Fig. 6D), and agrees with published rates (Dwyer et al., 2001). Furthermore, CHE-11::GFP (an IFT-A protein) moved anterogradely along dendrites at  $\sim 0.74$   $\mu\text{m}/\text{second}$ , which is also in agreement with published rates (Signor et al., 1999), and which is slower than ODR-10 and RAB-8 speeds (Fig. 6D). Together, these data suggest that RAB-8 and ODR-10, but not IFT proteins occupy the same dendritic transport carriers. To further test this idea, we performed time-lapse videomicroscopy on PHA/B dendrites in worms expressing *gfp::rab-8* and *odr-10::dsRed* transgenes. Using an Optosplit<sup>TM</sup> beam splitter to simultaneously acquire green and red signals, both ODR-10 and RAB-8 were detected in moving particles

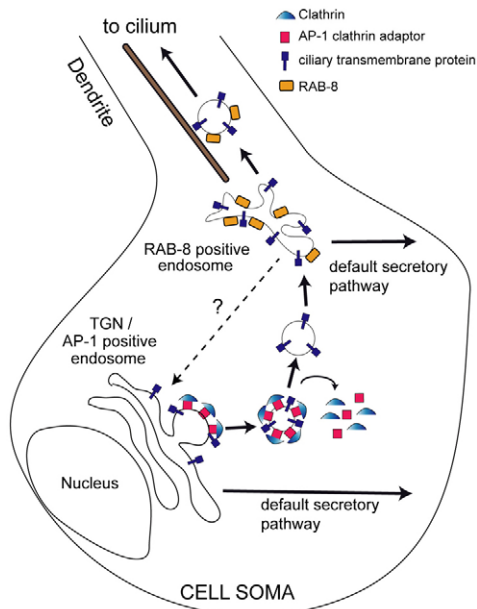


**Fig. 7. Model of AP-1/RAB-8 function in sorting ciliary membrane proteins in *C. elegans* sensory neurons.** In wt neurons, default or constitutive secretory pathways are proposed to target membrane proteins to all plasma membrane destinations. Ciliary transmembrane proteins are rescued from these pathways by AP-1 and RAB-8 activities functioning at distinct cell soma compartments. Initial budding of cilium-destined vesicles probably occurs at TGN/AP-1-positive endosomes, in a clathrin-dependent manner, followed by rapid uncoating of vesicles, and subsequent fusion with RAB-8-positive compartments. RAB-8 then facilitates formation of vesicles destined for dendrites and cilia. RAB-8 probably serves several roles in the delivery of ciliary proteins and membrane, both in the cell soma and in dendrites. Although ciliary membrane is likely to flow from TGN/AP-1-positive endosomes to RAB-8-positive endosomes, the involvement of a reverse retrograde trafficking route (question mark) is also possible.

in PHA/B dendrites (Fig. 6E,F). Kymographs showed that ~50% (anterograde) and ~55% (retrograde) of moving ODR-10 particles were RAB-8 positive, whereas ~25% (anterograde) and ~15% (retrograde) of moving RAB-8 particles were ODR-10 positive (Fig. 6G).

Together, our findings show that in the cell soma, ODR-10 and RAB-8, but not AP-1, localise to the same subcellular compartments. In addition, RAB-8 and ODR-10 display dynamic translocation properties in cell somas and dendrites, with the majority of ODR-10-associated vesicles positive for RAB-8.

## Discussion

### A conserved role for AP-1 complexes in defining the cilium compartment

Our findings support a conserved role for AP-1 in metazoan cilium integrity. In *C. elegans unc-101* ( $\mu 1$ ) and *aps-1* ( $\sigma 1$ ) disrupted animals, cilia lack distal regions, are disoriented at dendrite tips and possess defects in microtubule number, organisation or stability. Similarly, RNAi knockdown of  $\gamma$ -adaptin in RPE1 cells yields cilia that are curly, mispositioned (relative to nucleus) and possess microtubule acetylation defects. AP-1 probably performs its ciliary functions in a cell-autonomous fashion, because transgenic expression of *unc-101*(wt) in ciliated cells rescues the cilium structure defects of *C. elegans unc-101* mutants. AP-1 ciliary

function appears to be clathrin dependent, because ODR-10 is similarly mislocalised to all plasma membrane destinations in *chc-1* and *unc-101* mutants, and both possess cilium length or shape defects. Consistent with our findings, flagellar defects are observed in unicellular *Trypanosoma* following clathrin RNAi knockdown (Hung et al., 2004).

Although ciliary phenotypes in AP-1-deficient nematode and mammalian cells are comparable, they are not identical; *C. elegans unc-101* mutant *aps-1*(RNAi) animals mutants have short cilia, whereas cilia in AP-1 $\gamma$ -depleted RPE1 cells are long and clathrin-depleted RPE1 cells show no obvious cilia defects (Molla-Herman et al., 2010) Such variations might be due to model differences (worms vs mammals; neurons vs epithelial cells). Nonetheless, these findings are consistent with defective cilia or flagella structures in  $\mu 1$  (*C. elegans*) and  $\sigma 1$  (unicellular *Leishmania*) mutants (Ou et al., 2007; Vince et al., 2008). Metazoan AP-1 therefore joins other membrane-trafficking components with ciliary roles, including Rabs (Rab8) and exocyst subunits (Mazelova et al., 2009b; Nachury et al., 2007; Yoshimura et al., 2007; Zuo et al., 2009).

### A role for AP-1 complexes in microtubule stability or modification?

Our observation of missing or disorganised ciliary microtubules in *unc-101* mutants, together with breaks in ciliary acetylated  $\alpha$ -tubulin staining in AP-1-depleted RPE1 cells, suggests possible roles for AP-1 complexes in stabilising microtubules. Consistent with this notion, AP-1 $\gamma$  interacts with microtubules and co-immunoprecipitates with microtubule-associated proteins (Orzech et al., 2001). Furthermore, ciliary microtubule acetylation defects are found in mammalian cells overexpressing Rab8(wt) or Rab8-GTP (Nachury et al., 2007), which is relevant to AP-1 based on our findings (discussed below) that AP-1 and RAB-8 function in a common ciliary membrane transport pathway in *C. elegans*. In addition, although defects in ciliary microtubule acetylation were not detected in AP-1 mutants (because *C. elegans* cilia are not acetylated), these worms possess elevated acetylated microtubule levels in non-ciliary regions of ALM mechanosensory neurons. Interestingly, ciliary microtubule polyglutamylation is normal in AP-1-depleted mammalian cells, indicating that a role for AP-1 in microtubule post-translational modification might be specific to acetylation. Although untested, AP-1 might facilitate the transport of acetylation machinery components to mammalian cilia.

### AP-1, ciliogenesis and intraflagellar transport

In *C. elegans* and mammalian AP-1-depleted cells, no IFT defects were observed, indicating that AP-1 does not grossly influence the IFT machinery. Instead, the ciliary defects of AP-1-depleted cells are probably involved in disruption of cargos and not machineries. Indeed, several odorant signaling proteins found in *C. elegans* cilia regulate cilium length, shape and size with no impact on IFT (Mukhopadhyay et al., 2008; Roayaie et al., 1998). Since targeting of one of these proteins (ODR-1) to cilia requires AP-1 (Dwyer et al., 2001), *unc-101* ciliary defects might arise from mistrafficking of many such signaling proteins. Whether IFT also transports ciliary membrane proteins with cilium modulatory properties is unknown; however, IFT proteins are required for the ciliary distribution of *C. elegans* PKD-2 and OSM-9, as well as mammalian PKD2 and CNGB1b, indicating that downstream targeting or sorting of some ciliary transmembrane proteins involves IFT proteins (Bae et al., 2006; Follit et al., 2006; Jenkins et al.,

2006; Qin et al., 2005; Tan et al., 2007). However, this might not be the case for all transmembrane proteins; for example, *C. elegans* ODR-10 targeting to AWB cilia was reported to require AP-1 complexes, but not IFT proteins (Dwyer et al., 2001). Therefore, the previously reported model that *C. elegans* AP-1 and IFT function at distinct transport steps (AP-1 upstream or earlier and IFT downstream or later) in facilitating PKD-2 trafficking to cilia (Bae et al., 2006) might not be true of all ciliary membrane proteins. In addition, because mammalian IFT20 influences PKD2 sorting at cis-Golgi membranes (Follit et al., 2006), IFT proteins might also operate in early transport steps. Interestingly, early sorting of ODR-10 (or RAB-8) does not require *ift-20* (supplementary material Fig. S14), or indeed other IFT or IFT-related genes (supplementary material Fig. S12B–D) (Dwyer et al., 2001), indicating that Golgi-associated ciliary transmembrane sorting roles for IFT-20 are lost in neurons (or *C. elegans*), or that such functions are specific to certain ciliary membrane proteins.

Intriguingly, in AP-1-depleted RPE1/MDCKII cells, we find no defects in ciliary targeting of transmembrane SMO, SST3R and CNGB1b (supplementary material Fig. S15, and data not shown). Indeed, our finding for CNGB1b is an example of a protein whose ciliary targeting requires IFT (Jenkins et al., 2006), but not AP-1. However, since AP-1-depleted cells possess cilium structure defects, ciliary membrane protein transport is probably somewhat affected in these cells. Perhaps the discrepancy between worm and mammalian data is due to experimental model considerations, such as incomplete AP-1 knockdown via RNAi, genetic redundancy and cell type differences.

### A *C. elegans* ciliary membrane trafficking pathway involving AP-1 and RAB-8

A number of our findings implicate RAB-8 in an AP-1-mediated ciliary membrane trafficking pathway in *C. elegans* sensory neurons. Similarly to AP-1 mutants, worms overexpressing RAB-8 (GTP-locked) possess truncated cilia (Fig. 5B) (Mukhopadhyay et al., 2008), display ODR-10::GFP mislocalisation to all plasma membranes, and fail to form dendritic ODR-10-associated vesicles. These results are consistent with roles for Rab8 in targeting fibrocystin to IMCD3 cilia (Follit et al., 2010) and for sorting Rhodopsin to the *Xenopus* photoreceptor connecting cilium (Moritz et al., 2001). Indeed, a common pathway for AP-1/RAB-8 in ciliary membrane transport is also consistent with selective regulation of AP-1B-dependent basolateral transport by Rab8 (Ang et al., 2003).

Our finding that ODR-10 colocalises with RAB-8 in the cell soma, but is adjacent to AP-1 and TGN compartments, indicates that AP-1 and RAB-8 regulate ciliary membrane sorting or trafficking from two distinct sites, and that ODR-10 and ciliary membrane moves quickly through AP-1 compartments, but accumulates at RAB-8 compartments. Similar findings were found for mammalian fibrocystin, which colocalises with RAB8 and endosomal markers (Follit et al., 2010), but not with TGN. Indeed, distinct RAB8 and AP-1 compartments are reported in mammalian cells, where Rab8 colocalisation frequency with AP-1 $\gamma$  is very low (Ang et al., 2003). That ODR-10-marked dendritic transport carriers frequently incorporate RAB-8 suggests additional downstream transport roles for RAB-8, perhaps by facilitation of membrane fusion events in dendrites or at the ciliary base. It is unlikely that AP-1 contributes significantly to downstream delivery because AP-1  $\mu$ 1 localisation is restricted to cell soma, and in agreement with expected rapid uncoating of CCVs, moving dendritic vesicles containing AP-1 are very rarely observed.

### Model of AP-1 and RAB-8 function in ciliary membrane transport

We propose a *C. elegans* sensory neuronal model where AP-1 and RAB-8 function at closely apposed TGN or endosomal sites in cell soma to mediate early sorting of ciliary membrane (Fig. 7). We suggest that default secretory pathways exist in neurons, which deliver proteins to all plasma membrane destinations. AP-1 and RAB-8 would therefore rescue ciliary membrane from these pathways by facilitating formation of vesicles destined for somatodendritic regions and the cilium (Fig. 7). Because mistrafficking occurs only when RAB-8 activity is GTP locked, RAB-8 activity levels probably determine which sorting pathway ciliary membrane proteins take. Although the order of AP-1 and RAB-8 activity is unknown, vesicle budding at TGN (which might require AP-1) probably occurs before endosomal sorting (which might require RAB-8). RAB-8 is also likely to facilitate downstream transport steps and indeed multiple roles for this G-protein might explain why two Rab8 isoforms exist in mammals: one in cilia (Rab8a) and the other in the cytoplasm (Rab8b) (Nachury et al., 2007; Yoshimura et al., 2007). A caveat for this model, which is mostly based on worm data, is that we have yet to observe protein-trafficking defects to cilia of AP-1-depleted mammalian cells (supplementary material Fig. S15). However, it is known that membrane exchange with cilia is disrupted in cells that overexpress Rab8 (Nachury et al., 2007); accordingly, Rab8 probably regulates the distribution of at least some ciliary proteins.

What is clear from worm and mammalian data, however, is that disruption of AP-1 and Rab8 leads to cilium structure defects. But how exactly is membrane transport linked to defining the ciliary compartment? The obvious answer is that membrane transport directly exchanges or recycles membrane with the cilium and, at least in some ciliary subtypes, this also regulates exchange of membrane proteins with cilium remodeling properties (e.g. *C. elegans* odorant signaling proteins). However, although IFT proteins appear to be unaffected in AP-1-disrupted cells, the possibility still exists that ciliary membrane transport driven by AP-1 and RAB-8 could subtly influence IFT functions such as cargo loading or unloading, and therefore could contribute partially to cilium formation. Indeed, because AP-1 interacts with endosomal rabaptin-5 (Shiba et al., 2002), which in turn interacts biochemically and genetically with zebrafish Rab8 via the IFT protein Elipsa/DYF-11 (Omori et al., 2008), Rab8 could link AP-1 and IFT-mediated transport. The challenge for future work will be to further tease apart ciliary membrane transport events and IFT with a view to finding out how these pathways are related and how they are distinct.

### Materials and Methods

#### *C. elegans* strains, alleles and transgenes

Nematode strains maintained, cultured and crossed at 20°C using standard techniques (Brenner, 1974). Strains and alleles: N2, *unc-101(sy108)*, *rab-8(tm2526)*, *che-1(b1025ts)*, *cltc-1(tm3288)*, *bbs-8(nx77)*, *grk-2(gk268)*, *klp-11(tm324)*, *osm-5(p813)*, *ift-20(gk548)*, *osm-3(p802)* and *che-2(e1033)*. Transcriptional transgenes: *kyls104[*str-1p::gfp*]*, *kyls136[*str-2p::gfp+lin-15(+)*]*, *kyls164[*gcy-5p::gfp*]*, *gmls13[*srb-6p::gfp+pRF4*]* and *pkls519[*gpa-6p::gfp*]*. Translational transgenes: N2; *oq85[*arl-13p::syn-16::dsred+pRF4*]*, *kyls53[*str-1p::odr-10::gfp*]*, *oyEx[*str-1p::rab-8(Q67L)DA*]*, *myEx10[*che-11::gfp+pRF4*]*, *mnlS17[*osm-6::gfp+unc-36(+)*]*, *ejEx[*kap-1::gfp+pRF4*]*, *ejEx[*osm-3::gfp+pRF4*]*, *myEx[*che-2::gfp+pRF4*]*, *ejEx[*dyf-1::gfp+pRF4*]*, *nxEx[*ift-20::gfp + dpy-5(+)*]*, *oqEx[*unc-101p::unc-101::gfp+pRF4*]*, *oqEx71[*arl-13p::unc-101::gfp+pRF4*]*, *oqEx70[*srb-6p::unc-101::gfp+pRF4*]*, *oqEx69[*unc-101p::apm-1::gfp+pRF4*]*, *oqEx64[*arl-13p::gfp::rab-8+pRF4*]*, *oqEx65[*arl-13p::rab-8::gfp+pRF4*]*, *oqEx66[*srb-6p::odr-10::dsRED+pRF4*]*, *oqEx68[*str-1p::dsRED::rab-8+pRF4*]*, *oqEx58[*arl-13::gfp+pRF4*]*.

### Plasmids and antibodies

Plasmid containing *vha-6pro::gfp::rab-8* was from Akihiro Harada, IMCR, Gunma University, Japan. Antibodies: IFT88 (from Bradley Yoder, University of Alabama, Birmingham, AL), IFT46 (from Frederic Mallein-Gerin, Institut de Biologie et Chimie des Protéines, University of Lyon, France),  $\sigma$ 1A (DE/1) (from Linda Traub, University of Pittsburgh, PA), Pericentrin (Abcam; ab2914), acetylated-tubulin (Sigma; 6-11B-1),  $\gamma$ 1 Ab (Sigma; 100.3), BBS1 (Santa Cruz; sc-49790), Alexa Fluor secondary antibodies (Molecular Probes),  $\alpha$ -tubulin (MBL), polyglutamylated tubulin (GT335; Bernard Eddé, CNRS, Montpellier, France).

### Generation of *C. elegans* fluorescent-protein-tagged constructs and transgenes

Fusion PCR (Hobert, 2002) was used to generate *unc-101p::unc-101::gfp*, *srb-6p::unc-101::gfp*, *arl-13p::unc-101::gfp*, *str-1p::gfp::rab-8*, *arl-13p::gfp::rab-8*, *arl-13p::rab-8::gfp*, *unc-101p::apm-1::gfp* and *srb-6p::odr-10::dsRed*. Fusion PCR was also used to generate *srb-6p::aps-1* (sense and antisense), *arl-13p::aps-1* (sense and antisense) and *srb-6p::unc-101* (sense and antisense) constructs for ciliated cell-specific RNAi. *C. elegans* genomic DNA was used to amplify 5' UTR (promoter) sequences for *unc-101p* (5600 bp), *srb-6p* (1300 bp), *str-1p* (1357 bp) and *arl-13p* (300 bp), the entire exonic/intronic sequence for *rab-8*, *unc-101* and *odr-10*, and exon-rich sense or antisense fragments for *aps-1* (nucleotides 36–763) and *unc-101* (nucleotides 935–3791) RNAi constructs. For *str-1p::gfp::rab-8* and *arl-13p::gfp::rab-8* constructs, the *gfp::rab-8* fragment was amplified from plasmids containing *vha-6pro::gfp::rab-8*. Primer sequences are available on request. All constructs were co-injected at 1–10 ng/ $\mu$ l with pRF4 (50 ng/ $\mu$ l).

### Transmission electron microscopy

TEM of amphid channel cilia was carried out as described previously (Cevik et al., 2010).

### *C. elegans* fluorescence microscopy and IFT dendritic compartment motility assays

Fluorescence microscopy and IFT transport assays were conducted as described previously (Cevik et al., 2010). For colocalisation and co-movement analysis, two-colour images or movies of fluorescently-tagged proteins (red and green) were captured with an iXon<sup>EM+</sup> DV885 EMCCD camera (Andor Technology), operating on a Nikon motorised inverted research microscope (Eclipse Ti-E), coupled to a spinning disk confocal head and green (488 nm) and red (561 nm) laser excitation. For time-lapse two-colour imaging, consecutive green and red images were taken at exposures ranging from 330–600 mseconds. For simultaneous dual wavelength imaging, an emission field splitter (Optosplit) was used.

### Immunostaining of microtubule post-translational modifications in *C. elegans*

Worm fixation, immunostaining of amphid neuronal cilia for polyglutamylated tubulin, acetylated  $\alpha$ -tubulin, and  $\alpha$ -tubulin, and image capture and analysis were performed as previously described (Kimura et al., 2010).

### RPE1 and MDCKII mammalian cell culture

hTERT-RPE1 cells (CLONTECH) was a gift from M. Bornens (Institut Curie, Paris, France) and were grown in DMEM-F12 (1:1) supplemented with 10% FBS for basic culture conditions. To induce ciliogenesis, cells were grown to confluence on coverslips in basic culture, then transferred in low serum medium (0.5% FBS) for 24 or 48 hours as previously described (Molla-Herman et al., 2008). MDCKII cells cultured as described previously (Jenkins et al., 2009).

### AP-1 $\gamma$ silencing in RPE1 cells and MDCKII cells

RPE1 transfections followed recommended FuGENE HD (Roche) transfection reagent procedures. Subconfluent RPE1 cells grown on coverslips were transfected and immediately transferred in low-serum conditions for 24 hours. For siRNA experiments, RPE1 cells were treated with 200 pmol control siRNA (Luciferase, siLuc; 5'-GCCATCTATCCTCTAGAGGATG-3') or siRNA targeting AP-1 complex ( $\gamma$ -adaptin, siAPI; 5'-GCGCCUGUACAAAGCAAUU-3') as previously described (Borck et al., 2008; Molla-Herman et al., 2008). MDCKII cells were stably transfected with short-hairpin RNA against AP-1 $\gamma$  [5'-GCGCTTGACAAAGCAATTC-3' (sense); 5'-TTCAAGAGAAGAATTGCTTTGTACAAGCGC-3' (antisense)], as described previously (Jenkins et al., 2009).

### RPE1 cells and MDCKII cell immunohistochemistry and fluorescence microscopy

RPE1 cells fixed and immunostained using standard procedures, and examined with epifluorescence microscopy (Leica) using a CCD camera (Princeton Instruments). Images were acquired with MetaMorph (Molecular Devices) and processed with MetaMorph and Photoshop CS2 (Adobe Systems). For 3D reconstruction, Z-stacked images were deconvolved with Metamorph and reconstructed with Imapris software (Bitplane). Reconstructed images were used to determine cilium length, cilium to adherent surface angle ( $\hat{A}$ ) and cilium distribution (relative to nucleus) as follows. Points corresponding to ciliary base and tip form a triangle with a third point corresponding to projection of tip on the x,y plane. In this triangle, the hypotenuse

is the cilium length. Z position of cilia tip (ZCT) and cilia base (ZCB) were calculated, and distance between these two (ZCT–ZCB) corresponds to opposite side of triangle (OS). Since  $\sin(\hat{A})=OS/CL$ ,  $\sin^{-1}$  values were calculated, obtaining angle ( $\hat{A}$ ). For cilium distribution, objects (nuclei and cilia) were defined in 3D images and centre of mass (CM) obtained for each. Cilium distribution values were calculated by comparing cilium and nucleus CMs.

MDCKII cell fixation and immunostaining was conducted using standard procedures. Fluorescence signals acquired under an Olympus Fluoview 500 confocal microscope and images were obtained by capturing a series of stacks every 0.5  $\mu$ m (generally 3–5  $\mu$ m) and combining images into a composite stack.

### Immunoblotting of RPE1 protein lysates

RPE1 cells were lysed in 0.02 M Tris-HCl pH 7.5, 1% (v/v) NP40, 0.1 M NH<sub>4</sub>SO<sub>4</sub>, 10% glycerol (v/v), 10 mM protease inhibitor cocktail (Sigma) for 30 minutes at 4°C. After centrifugation (12,000 r.p.m. for 30 minutes at 4°C), cleared lysates were separated by SDS-PAGE and transferred onto PVDF membrane. Immunoblotting performed using the indicated primary antibodies and revealed using ECL+ Detection Kit (GE Healthcare).

The authors acknowledge no conflict of interest. We thank the *Caenorhabditis* Genetics Center, Japanese Bioresource Project, B. Grant, A. Harada and P. Sengupta for constructs/strains, and UCD Conway Institute imaging facility for assistance. Research was funded by Science Foundation of Ireland President of Ireland Young Researcher Award (O.E.B.), and grants from ANR 'GENOPAT 2009' (A.B.), JSPS Wakate S (M.S) and NIH (R01DC009606; J.R.M.). Deposited in PMC for release after 12 months.

Supplementary material available online at

<http://jcs.biologists.org/cgi/content/full/123/22/3966/DC1>

### References

- Ang, A. L., Folsch, H., Koivisto, U. M., Pypaert, M. and Mellman, I. (2003). The Rab8 GTPase selectively regulates AP-1B-dependent basolateral transport in polarized Madin-Darby canine kidney cells. *J. Cell Biol.* **163**, 339–350.
- Badano, J. L., Mitsuma, N., Beales, P. L. and Katsanis, N. (2006). The ciliopathies: an emerging class of human genetic disorders. *Annu. Rev. Genomics Hum. Genet.* **7**, 125–148.
- Bae, Y. K., Qin, H., Knobel, K. M., Hu, J., Rosenbaum, J. L. and Barr, M. M. (2006). General and cell-type specific mechanisms target TRPP2/PKD-2 to cilia. *Development* **133**, 3859–3870.
- Blacque, O. E. and Leroux, M. R. (2006). Bardet-Biedl syndrome: an emerging pathomechanism of intracellular transport. *Cell. Mol. Life Sci.* **63**, 2145–2161.
- Blacque, O. E., Perens, E. A., Borojevich, K. A., Inglis, P. N., Li, C., Warner, A., Khattri, J., Holt, R. A., Ou, G., Mah, A. K. et al. (2005). Functional genomics of the cilium, a sensory organelle. *Curr. Biol.* **15**, 935–941.
- Blacque, O. E., Cevik, S. and Kaplan, O. I. (2008). Intraflagellar transport: from molecular characterisation to mechanism. *Front. Biosci.* **13**, 2633–2652.
- Borck, G., Molla-Herman, A., Boddaert, N., Encha-Razavi, F., Philippe, A., Robel, L., Desguerre, I., Brunelle, F., Benmerah, A., Munnich, A. et al. (2008). Clinical, cellular, and neuropathological consequences of AP1S2 mutations: further delineation of a recognizable X-linked mental retardation syndrome. *Hum. Mutat.* **29**, 966–974.
- Brenner, S. (1974). The genetics of *Caenorhabditis elegans*. *Genetics* **77**, 71–94.
- Cevik, S., Hori, Y., Kaplan, O. I., Kida, K., Toivenon, T., Foley-Fisher, C., Cottell, D., Katada, T., Kontani, K. and Blacque, O. E. (2010). Joubert syndrome Arl13b functions at ciliary membranes and stabilizes protein transport in *Caenorhabditis elegans*. *J. Cell Biol.* **188**, 953–969.
- Chun, D. K., McEwen, J. M., Burbea, M. and Kaplan, J. M. (2008). UNC-108/Rab2 regulates postendocytic trafficking in *Caenorhabditis elegans*. *Mol. Biol. Cell* **19**, 2682–2695.
- Deretic, D., Huber, L. A., Ransom, N., Mancini, M., Simons, K. and Papermaster, D. S. (1995). rab8 in retinal photoreceptors may participate in rhodopsin transport and in rod outer segment disk morphogenesis. *J. Cell Sci.* **108**, 215–224.
- Dwyer, N. D., Troemel, E. R., Sengupta, P. and Bargmann, C. I. (1998). Odorant receptor localization to olfactory cilia is mediated by ODR-4, a novel membrane-associated protein. *Cell* **93**, 455–466.
- Dwyer, N. D., Adler, C. E., Crump, J. G., L'Etoile, N. D. and Bargmann, C. I. (2001). Polarized dendritic transport and the AP-1 mu1 clathrin adaptor UNC-101 localize odorant receptors to olfactory cilia. *Neuron* **31**, 277–287.
- Eggenchwiler, J. T. and Anderson, K. V. (2007). Cilia and developmental signaling. *Annu. Rev. Cell Dev. Biol.* **23**, 345–373.
- Esposito, G., Di Schiavi, E., Bergamasco, C. and Bazzicalupo, P. (2007). Efficient and cell specific knock-down of gene function in targeted *C. elegans* neurons. *Gene* **395**, 170–176.
- Follit, J. A., Tuft, R. A., Fogarty, K. E. and Pazour, G. J. (2006). The intraflagellar transport protein IFT20 is associated with the Golgi complex and is required for cilia assembly. *Mol. Biol. Cell* **17**, 3781–3792.
- Follit, J. A., Li, L., Vucica, Y. and Pazour, G. J. (2010). The cytoplasmic tail of fibrocystin contains a ciliary targeting sequence. *J. Cell Biol.* **188**, 21–28.

- Folsch, H., Ohno, H., Bonifacino, J. S. and Mellman, I. (1999). A novel clathrin adaptor complex mediates basolateral targeting in polarized epithelial cells. *Cell* **99**, 189–198.
- Hinrichsen, L., Harborth, J., Andrees, L., Weber, K. and Ungewickell, E. J. (2003). Effect of clathrin heavy chain- and alpha-adaptin-specific small inhibitory RNAs on endocytic accessory proteins and receptor trafficking in HeLa cells. *J. Biol. Chem.* **278**, 45160–45170.
- Hobert, O. (2002). PCR fusion-based approach to create reporter gene constructs for expression analysis in transgenic *C. elegans*. *Biotechniques* **32**, 728–730.
- Hung, C. H., Qiao, X., Lee, P. T. and Lee, M. G. (2004). Clathrin-dependent targeting of receptors to the flagellar pocket of procyclic-form *Trypanosoma brucei*. *Eukaryotic Cell* **3**, 1004–1014.
- Hunt-Newbury, R., Viveiros, R., Johnsen, R., Mah, A., Anastas, D., Fang, L., Halfnight, E., Lee, D., Lin, J., Lorch, A. et al. (2007). High-throughput in vivo analysis of gene expression in *Caenorhabditis elegans*. *PLoS Biol.* **5**, e237.
- Jenkins, P. M., Hurd, T. W., Zhang, L., McEwen, D. P., Brown, R. L., Margolis, B., Verhey, K. J. and Martens, J. R. (2006). Ciliary targeting of olfactory CNG channels requires the CNGB1b subunit and the kinesin-2 motor protein, KIF17. *Curr. Biol.* **16**, 1211–1216.
- Jenkins, P. M., Zhang, L., Thomas, G. and Martens, J. R. (2009). PACS-1 mediates phosphorylation-dependent ciliary trafficking of the cyclic-nucleotide-gated channel in olfactory sensory neurons. *J. Neurosci.* **29**, 10541–10551.
- Kimura, Y., Kurabe, N., Ikegami, K., Tsutsumi, K., Konishi, Y., Kaplan, O. I., Kunitomo, H., Iino, Y., Blacque, O. E. and Setou, M. (2010). Identification of tubulin deglutamylase among *Caenorhabditis elegans* and mammalian cytosolic carboxypeptidases (CCPs). *J. Biol. Chem.* **285**, 22936–22941.
- Lee, J., Jongeward, G. D. and Sternberg, P. W. (1994). *unc-101*, a gene required for many aspects of *Caenorhabditis elegans* development and behavior, encodes a clathrin-associated protein. *Genes Dev.* **8**, 60–73.
- Mazelova, J., Astuto-Gribble, L., Inoue, H., Tam, B. M., Schonteich, E., Prekeris, R., Moritz, O. L., Randazzo, P. A. and Deretic, D. (2009a). Ciliary targeting motif VxPx directs assembly of a trafficking module through Arf4. *EMBO J.* **28**, 183–192.
- Mazelova, J., Ransom, N., Astuto-Gribble, L., Wilson, M. C. and Deretic, D. (2009b). Syntaxin 3 and SNAP-25 pairing, regulated by omega-3 docosahexaenoic acid, controls the delivery of rhodopsin for the biogenesis of cilia-derived sensory organelles, the rod outer segments. *J. Cell Sci.* **122**, 2003–2013.
- Molla-Herman, A., Boullaran, C., Ghossoub, R., Scott, M. G., Burtey, A., Zarka, M., Saunier, S., Concordet, J. P., Marullo, S. and Benmerah, A. (2008). Targeting of beta-arrestin2 to the centrosome and primary cilium: role in cell proliferation control. *PLoS ONE* **3**, e3728.
- Molla-Herman, A., Ghossoub, R., Blisnick, T., Meunier, A., Serres, C., Silbermann, F., Emmerson, C., Romeo, K., Bourdoncle, P., Schmitt, A., Saunier, S., Spassky, N., Bastin, P. and Benmerah, A. (2010). The ciliary pocket: an endocytic membrane domain at the base of primary and motile cilia. *J. Cell Sci.* **123**, 1785–1795.
- Moritz, O. L., Tam, B. M., Hurd, L. L., Peranen, J., Deretic, D. and Papermaster, D. S. (2001). Mutant rab8 impairs docking and fusion of rhodopsin-bearing post-Golgi membranes and causes cell death of transgenic *Xenopus* rods. *Mol. Biol. Cell* **12**, 2341–2351.
- Motley, A., Bright, N. A., Seaman, M. N. and Robinson, M. S. (2003). Clathrin-mediated endocytosis in AP-2-depleted cells. *J. Cell Biol.* **162**, 909–918.
- Mukhopadhyay, S., Lu, Y., Shaham, S. and Sengupta, P. (2008). Sensory signaling-dependent remodeling of olfactory cilia architecture in *C. elegans*. *Dev. Cell* **14**, 762–774.
- Nachury, M. V., Loktev, A. V., Zhang, Q., Westlake, C. J., Peranen, J., Merdes, A., Slusarski, D. C., Scheller, R. H., Bazan, J. F., Sheffield, V. C. et al. (2007). A core complex of BBS proteins cooperates with the GTPase Rab8 to promote ciliary membrane biogenesis. *Cell* **129**, 1201–1213.
- Omori, Y., Zhao, C., Saras, A., Mukhopadhyay, S., Kim, W., Furukawa, T., Sengupta, P., Veraksa, A. and Malicki, J. (2008). Elipsa is an early determinant of ciliogenesis that links the IFT particle to membrane-associated small GTPase Rab8. *Nat. Cell Biol.* **10**, 437–444.
- Orzech, E., Livshits, L., Leyt, J., Okhrimenko, H., Reich, V., Cohen, S., Weiss, A., Melamed-Book, N., Lebendiker, M., Altschuler, Y. et al. (2001). Interactions between adaptor protein-1 of the clathrin coat and microtubules via type Ia microtubule-associated proteins. *J. Biol. Chem.* **276**, 31340–31348.
- Ou, G., Koga, M., Blacque, O. E., Murayama, T., Ohshima, Y., Schafer, J. C., Li, C., Yoder, B. K., Leroux, M. R. and Scholey, J. M. (2007). Sensory ciliogenesis in *Caenorhabditis elegans*: assignment of IFT components into distinct modules based on transport and phenotypic profiles. *Mol. Biol. Cell.* **18**, 1554–1569.
- Qin, H., Diener, D. R., Geimer, S., Cole, D. G. and Rosenbaum, J. L. (2004). Intraflagellar transport (IFT) cargo: IFT transports flagellar precursors to the tip and turnover products to the cell body. *J. Cell Biol.* **164**, 255–266.
- Qin, H., Burnette, D. T., Bae, Y. K., Forscher, P., Barr, M. M. and Rosenbaum, J. L. (2005). Intraflagellar transport is required for the vectorial movement of TRPV channels in the ciliary membrane. *Curr. Biol.* **15**, 1695–1699.
- Roayaie, K., Crump, J. G., Sagasti, A. and Bargmann, C. I. (1998). The G alpha protein ODR-3 mediates olfactory and nociceptive function and controls cilium morphogenesis in *C. elegans* olfactory neurons. *Neuron* **20**, 55–67.
- Shiba, Y., Takatsu, H., Shin, H. W. and Nakayama, K. (2002). Gamma-adaptin interacts directly with Rabaptin-5 through its ear domain. *J. Biochem.* **131**, 327–336.
- Signor, D., Wedaman, K. P., Orozco, J. T., Dwyer, N. D., Bargmann, C. I., Rose, L. S. and Scholey, J. M. (1999). Role of a class DHC1b dynein in retrograde transport of IFT motors and IFT raft particles along cilia, but not dendrites, in chemosensory neurons of living *Caenorhabditis elegans*. *J. Cell Biol.* **147**, 519–530.
- Tan, P. L., Barr, T., Inglis, P. N., Mitsuma, N., Huang, S. M., Garcia-Gonzalez, M. A., Bradley, B. A., Coforio, S., Albrecht, P. J., Watnick, T. et al. (2007). Loss of Bardet Biedl syndrome proteins causes defects in peripheral sensory innervation and function. *Proc. Natl. Acad. Sci. USA* **104**, 17524–17529.
- Traub, L. M. (2009). Tickets to ride: selecting cargo for clathrin-regulated internalization. *Nat. Rev. Mol. Cell Biol.* **10**, 583–596.
- Troemel, E. R., Chou, J. H., Dwyer, N. D., Colbert, H. A. and Bargmann, C. I. (1995). Divergent seven transmembrane receptors are candidate chemosensory receptors in *C. elegans*. *Cell* **83**, 207–218.
- Vieira, O. V., Gaus, K., Verkade, P., Fullekrug, J., Vaz, W. L. and Simons, K. (2006). FAPP2, cilium formation, and compartmentalization of the apical membrane in polarized Madin-Darby canine kidney (MDCK) cells. *Proc. Natl. Acad. Sci. USA* **103**, 18556–18561.
- Vince, J. E., Tull, D. L., Spurck, T., Derby, M. C., McFadden, G. I., Gleeson, P. A., Gokool, S. and McConville, M. J. (2008). Leishmania adaptor protein-1 subunits are required for normal lysosome traffic, flagellum biogenesis, lipid homeostasis, and adaptation to temperatures encountered in the mammalian host. *Eukaryotic Cell* **7**, 1256–1267.
- Yoshimura, S., Egerer, J., Fuchs, E., Haas, A. K. and Barr, F. A. (2007). Functional dissection of Rab GTPases involved in primary cilium formation. *J. Cell Biol.* **178**, 363–359.
- Zuo, X., Guo, W. and Lipschutz, J. H. (2009). The exocyst protein Sec10 is necessary for primary ciliogenesis and cystogenesis in vitro. *Mol. Biol. Cell* **20**, 2522–2529.